Neurobiology of Disease 132 (2019) 104584

Contents lists available at ScienceDirect

Neurobiology of Disease

journal homepage: www.elsevier.com/locate/ynbdi

# Smooth muscle cell-specific knockout of FBW7 exacerbates intracranial atherosclerotic stenosis

Yan Shen[a,1], Xiufen Chen[a,1], Chunling Chi[a], Han Wang[b], Jun Xue[c], Danying Su[a], Hongwei Wang[d], Meng Li[e], Bin Liu[a,*], Qi Dong[f,*]

[a] Department of Neurology, The Fourth Affiliated Hospital of Harbin Medical University, Harbin, China
[b] Department of Hand and Foot Surgery, Dalian Friendship Hospital, Dalian, China
[c] Department of Neurology, Dalian Friendship Hospital, Dalian, China
[d] Department of Minimally Invasive Neurosurgery, The Fourth Affiliated Hospital of Harbin Medical University, Harbin, China
[e] Department of Cardiology, The Fourth Affiliated Hospital of Harbin Medical University, Harbin, China
[f] Department of Neurology, The First Affiliated Hospital of Harbin Medical University, Harbin, China

ARTICLE INFO

*Keywords:*
FBW7
Oxidative stress
NADPH oxidase
Nox1
Smooth muscle cells
Intracranial atherosclerotic stenosis

ABSTRACT

Intracranial atherosclerotic stenosis (ICAS), the most common cause of stroke worldwide, is associated with high risk of recurrent ischemic stroke. F-box and WD repeat domain containing protein 7 (FBW7), an ubiquitin E3 ligase, is recently suggested to be involved in atherogenesis. However, whether FBW7 affects cerebrovascular remodeling during ICAS remains unknowns. We found that the expression of FBW7 was decreased in mouse brain microvessels from high-fat diet (HFD)-fed atherosclerotic mice. The reduced FBW7 expression was negatively associated with the remodeling of middle cerebral artery (MCA). Specific loss of FBW7 in smooth muscle cells (SMCs) markedly potentiated brain vascular SMC (VSMC) proliferation, migration and subsequent MCA remodeling in atherosclerotic mice. The increase of total reactive oxygen species (ROS) generation and nicotinamide adenine dinucleotide phosphate (NADPH) oxidase activity in brain microvessels and VSMCs were enhanced after knockout of FBW7, while the mitochondria-derived ROS was unchanged. Analysis of several key subunits of NADPH oxidase revealed that FBW7 deficiency augmented HFD-induced the increase of Nox1 expression, but had no effect on p47phox and p67phox phosphorylation as well as p22phox expression. Both NADPH oxidase specific inhibitor and Nox1 downregulation abrogated the effects of FBW7 deficiency on MCA remodeling. Immunoprecipitation assay identified that FBW7 interacted with Nox1. FBW7 knockout increased Nox1 protein stability by inhibiting ubiquitin-mediated degradation. Collectively, our study demonstrates that SMC-specific deficiency of FBW7 exacerbates ICAS by facilitating Nox1-derived ROS generation, VSMC proliferation and cerebrovascular remodeling.

## 1. Introduction

Intracranial atherosclerotic stenosis (ICAS) involving major cerebral arteries is one of the most common causes of stroke worldwide and is also associated with higher risk of recurrent ischemic stroke than other subtypes of stroke (Gorelick et al., 2008). The middle cerebral artery (MCA) is the most common site suffering from narrowing, followed by the internal carotid artery, basilar artery, and intracranial vertebral artery (Chimowitz et al., 2005; Chimowitz et al., 2011). ICAS has been found to be highly prevalent in Asian, African-American and Hispanic population (Gorelick et al., 2008). This suggests that the global stroke burden from ICAS may continue to grow because these populations are major drivers of global population growth. Thus, an understanding of ICAS pathophysiology and effective treatment options are constantly needed. Recently, Zhang et al. showed that cerebrovascular remodeling was the major pathogenesis of intracranial stenosis because they observed inward narrowing of MCA by high-resolution MRI (HR-MRI) (Zhang et al., 2019a). In fact, it has been demonstrated a close relationship between MCA remodeling patterns and ischemic stroke (Zhang et al., 2017). Notably, vascular smooth muscle cell (VSMC) proliferation in medium and migration into intima are indispensable for vascular remodeling (Dzau et al., 2002), indicating inhibition of

* Corresponding author at: Department of Neurology, The Fourth Affiliated Hospital of Harbin Medical University, 37 Yiyuan Rd, Nangang Region, Heilongjiang, Harbin 150001, China.
*E-mail addresses:* kevinliu_hmu@sina.com (B. Liu), HP_Jeanne@163.com (Q. Dong).
[1] Yan Chen and Xiufen Chen contributed equally to this work.

https://doi.org/10.1016/j.nbd.2019.104584
Received 16 April 2019; Received in revised form 26 July 2019; Accepted 20 August 2019
Available online 21 August 2019
0969-9961/ 

cerebrovascular remodeling may be a therapeutic approach to decrease the prevalence of ICAS.

Oxidative stress resulting from excessive reactive oxygen species (ROS) generation plays a key role in atherosclerotic pathogenesis (Han et al., 2017; Wu et al., 2018). ROS is mainly derived from nicotinamide adenine dinucleotide phosphate (NADPH) oxidase and mitochondrial ROS (mROS) (Forstermann, 2008). It initially induces endothelial injury, VSMC proliferation and migration, and macrophages recruitment, leading to plaque formation (Han et al., 2017; Wu et al., 2018). Although ROS acts at multiple steps, it has been heavily implicated in VSMC activation and vascular remodeling (Dzau et al., 2002; Zhao et al., 2015; Shen et al., 2018). Multiple studies have clearly showed that reduced ROS generation could markedly inhibit VSMC proliferation and remodeling in pulmonary artery, thoracic aorta and cerebral vessel (Chen et al., 2019; Fois et al., 2018; Dong et al., 2019). Despite several mechanisms for ROS generation have been identified, such as NADPH oxidase activation and mitochondrial dysfunction (Zhao et al., 2015; Dong et al., 2019; Prentice et al., 2015), the regulation of ROS generation in VSMCs is still unclear.

Protein degradation plays a critical role in a variety of cellular functions (Ciechanover et al., 2000; Wang et al., 2018). F-box and WD repeat domain containing protein 7 (FBW7) is a type of SCF E3 ubiquitin ligases that regulates protein substrates by post-translational modification (Biswas et al., 2011). It is associated with targeting several mammalian oncoproteins for degradation, such as c-jun, c-myc, cyclin E and Notch (Biswas et al., 2011; Tang et al., 2011; Yada et al., 2004). Davis et al. revealed that FBW7 shifted cancer cell oxidative metabolism, leading to context-specific metabolic vulnerabilities (Davis et al., 2018). Global knockout of FBW7 resulted in defective vascular development (Tsunematsu et al., 2004; Tetzlaff et al., 2004), indicating a vital role of FBW7 in cardiovascular system. More importantly, a recent study showed that a pro-atherosclerotic factor oxidized low density lipoprotein decreased FBW7 expression and attenuated FBW7-mediated KLF15 degradation, whereas specific loss of KLF15 in VSMCs prevented atherosclerotic development (Zheng et al., 2018). However, the direct role in FBW7 in atherogenesis, particularly in ICAS, has not been addressed. The aim of this study is to investigate the involvement of FBW7 in the pathogenesis of ICAS, and further clarify its role in oxidative stress-mediated VSMC proliferation. Our results suggest that FBW7 is an important regulator in cerebrovascular remodeling.

## 2. Methods and materials

### 2.1. Materials and reagents

Adenovirus targeting Nox1 siRNA (Ad-siNox1) and its negative control (Ad-GFP) were purchased from Cyagen (CA, USA). Dulbecco's modified Eagle's medium (DMEM), fetal bovine serum (FBS), penicillin, streptomycin and collagenases were obtained from Invitrogen (CA, USA). Apocynin, bromodeoxyuridine (BrdU) antibody, hematoxylin and eosin solution, rabbit anti-mouse-cy3 antibody, Oil Red O, 2′,7′-dichlorofluorescin diacetate ($H_2$DCF-DA), dihydroethidium (DHE), MitoSOX Red, NADPH, lucigenin and cycloheximide were obtained from Sigma-Aldrich (MO, USA).

### 2.2. Animal model

FBW7-floxed mice ($FBW7^{f/f}$) were generated and obtained by Cyagen. To obtain smooth muscle cell (SMC)-specific knockout mice ($FBW7^{SMCKO}$), the floxed FBW7 allele were crossed with SM22α-Cre mice (Jackson Laboratory, ME, USA). Genotyping was performed by PCR using the primers that target wild-type allele, the floxed allele and cre recombinase (Fig. S1). After genotyping analysis, $FBW7^{f/f}$ and $FBW7^{SMCKO}$ littermates were used as breeding pairs to further generate the $FBW7^{f/f}$ ApoE−/− and $FBW7^{SMCKO}$ $ApoE^{-/-}$ littermates used in this study. At the age of 8 weeks, the mice were administrated with either a low fat diet (LFD) or a high fat diet (HFD) (60% of calories from fat, D12492, Research Diets, Inc., NJ, USA) for 32 weeks. All animals were randomly divided into 8 groups ($n$ = 20/per group): $FBW7^{f/f}$ LFD, $FBW7^{SMCKO}$ LFD, $FBW7^{f/f}$ HFD, $FBW7^{SMCKO}$ HFD, $FBW7^{SMCKO}$ HFD vehicle, $FBW7^{SMCKO}$ HFD apocynin, $FBW7^{SMCKO}$ HFD Ad-GFP and $FBW7^{SMCKO}$ HFD Ad-siNox1. Apocynin in DMSO (vehicle) was injected intraperitoneally after 6-week HFD administration, and then continuously dosed every other day. On the basis of the data from previous studies (Zhang et al., 2019b; Qiu et al., 2016), the dosage for a body weight of 5 mg/kg was chosen. For adenovirus delivery, after 24 weeks of HFD treatment, mice were injected with $5.0 \times 10^{10}$ vp of Ad-GFP or Ad-siNox1 via tail vein. The adenovirus injection repeated weekly for 8 weeks. All animals were sacrificed 32 weeks after a HFD treatment. The animal protocols were carried out according to the institutional guidelines from the Principles of Laboratory Animal Care of Harbin Medical University and were approved by the Harbin Medical University Institutional Animal Ethics Committee.

### 2.3. Isolation of mouse brain microvessels and VSMCs

The brain microvessels and mouse brain VSMCs (MBVSMCs) were isolated as previously described with some modifications (Shen et al., 2018; Gauthier et al., 2012). In brief, the brain was removed and homogenized in ice-cold sucrose buffer (0.32 mol/L sucrose, 3 mmol/L HEPES, and pH 7.4) followed by centrifugation at 4 °C for 10 min at 1000*g*. The supernatant and the dense white layer of myelin in the upper part of the pellet were discarded. The pellet was re-suspended in ice-cold sucrose buffer followed by centrifugation at 4 °C for 10 min at 1000*g*. This step was repeated twice. The final pellet was suspended in phosphate-buffered saline +0.1% bovine plasma albumin in PBS, centrifuged at 14,000*g* and the precipitate was microvessels. The pellet with vessels were further re-suspended in DMEM containing 10% FBS, 100 U/mL penicillin, 100 U/mL streptomycin and 0.05% collagenases, and incubated for 3 h in a 37 °C water bath. An equal volume of ice-cold complete DMEM supplemented with 5 mmol/L EDTA was added followed by centrifugation at room temperature for 12 min at 1000*g*. After removing the supernatant, the pellet was re-suspended in complete DMEM at 37 °C and seeded in sterile cell culture plate at 37 °C in 5% $CO_2$ atmosphere. MBVSMCs were passaged every 5–8 days using 0.25% trypsin. In this study, all cells were used within 3 passages.

### 2.4. Histological analysis

Animals were sacrificed by cardiac perfusion with phosphate buffer followed by 4% paraformaldehyde under anesthesia with isoflurane. The 4-μm sections of MCA, cut at the level above the inferior horn of the lateral ventricles, were stained with hematoxylin and eosin for histopathological examination by a light microscope (CKX41, Olympus, Tokyo, Japan). The medial cross sectional area (CSA) was obtained as: $CSA = (\pi/4) \times (De^2 - Di^2)$. De and Di represented the external and internal diameter, which were calculated as external elastic lamina circumferences/π and internal elastic lamina circumferences/π, respectively. The circumferences were measured by ImageJ software (National Institutes of Health, Maryland, USA). For immunochemical staining of FBW7, the sections were blocked with 5% normal goat serum (Zhongshan Jinqiao Bio-Technology Co. Ltd., Beijing, China) followed by incubation of FBW7 antibody (1:100, Abcam, MA, USA) overnight. After washing with PBS for 3 times, the sections were incubated with biotinylated secondary antibody (BioVision, CA, USA). The expression of FBW7 was visualized with the streptavidin-perosidase reaction using 3,3′-diaminobenzidine under a light microscope (CKX41). Immunofluorescence of α-SMA was performed by incubation with α-SMA antibody (1:200, Santa Cruz, CA, USA) overnight at 4 °C. The sections were then incubated with rabbit anti-mouse-Cy3 (1:100) for 1 h at room temperature. Immunofluorescence was observed with a confocal system (FV1000, Olympus). The sections were stained with Oil

Red O to observe lipid accumulation in MCA.

### 2.5. Blood measurement

Systemic blood samples were harvested at the end of 32-week of HFD treatment followed by centrifugation at room temperature for 10 min at 1000*g*. The plasma was taken for analysis of triglyceride (TG), low-density lipoprotein (LDL), cholesterol (CHO) and high-density lipoprotein (HDL) using commercial kits (all from Jian Cheng Biological Engineering Institute, Nanjing, China) according to manufacturer's instructions.

### 2.6. Oxidative stress level measurement

Brain microvessels or MBVSMCs isolated from each group were homogenized at the end of experiment. The concentration of malondialdehyde (MDA), glutathion peroxidase (GPx) and superoxide dismutase (SOD) in homogenate were determined by commercial kits according supplier's instructions (Nanjing Jiancheng Bioengineering Institute, Nanjing, China). For the determination of total reactive oxygen species (ROS) generation, MCA sections or MBVSMCs were incubated with $H_2$DCF-DA (10 μmol/L) for 30 min at 37 °C in dark. After washing with PBS, the images were captured with a confocal system. Superoxide anion ($O_2^-$) generation was visualized by DHE (5 μmol/L) staining. Following 30 min incubation, the sections or MBVSMCs were observed under a confocal microscope. To test the generation of mitochondrial ROS (mROS), the sections or MBVSMCs were incubated with MitoSOX Red (5 μmol/L) in the dark at 37 °C for 30 min and detected with a confocal microscope. The fluorescence intensity was quantified with ImageJ software. NADPH oxidase activity was determined by a lucigenin-enhanced chemiluminescence assay as described previously (Zhao et al., 2015; Noubade et al., 2014). The homogenates were then centrifuged at 12000 ×*g* for 5 min. The lucigenin (5 mmol/L) was added to the supernatant and incubated for 10 min at 37 °C in the dark. Basal relative light units (RLUs) of chemiluminescence were obtained with a luminometer (Promega, WI, USA). The experimental RLU was obtained by adding NADPH (100 μmol/L) and recorded every 15 s for 20 min. The NADPH oxidase activity was calculated as (total experimental RLU − total basal RLU)/ (20 × 60s)/ total protein concentration.

### 2.7. Western blot analysis and immunoprecipitation

Brain microvessels or MBVSMCs were harvested and lysed in a lysis buffer containing 50 mmol/L HEPES (Promocell, Heidlberg, Germany), 1% Triton X100, and protease and phosphatase inhibitors (Pierce Biotechnology, IL, USA). The cellular protein concentration was determined by a bicinchoninic acid kit (BioRad, CA, USA). The samples containing equal protein were separated by sodium dodecyl sulphate polyacrylamide gel electrophoresis (SDS-PAGE) on 8%–10% gels. The separated proteins were then transferred onto nitrocellulose membranes (Millipore, MA, USA). The membranes were blocked with 5% non-fat milk in TBST (in mmol/L, 10 Tris-HCl, 150 NaCl, 0.05% Tween-20, pH 7.6) and probed with the following primary antibodies at 4 °C overnight: FBW7 (1:500), Nox1 (1:1000) (Abcam), p22hox (1:1000), GAPDH (1:2000) (Santa Cruz), p-p47phox, p47phox, p67phox, p67phox and ubiquitin (1:1000) (Cell Signaling Technology, MA, USA). After washing with TBST three times, the blots were incubated with HRP-conjugated secondary antibodies (1:1000, Cell Signaling Technology) and then exposed to enhanced chemiluminescence kit according the manufacturer's instructions (Thermo Fisher Scientific Inc., IL, USA). Densitometric analysis was performed using ImageJ software. For immunoprecipitation, equal cellular proteins were incubated with limiting amounts of indicated antibodies overnight at 4 °C with constant rotation. The complexes were collected following incubation with protein A/G agarose beads for 4 h at 4 °C and resuspended in RIPA lysis buffer for western blot analysis using corresponding antibodies.

### 2.8. Real-time PCR

The total RNA from brain microvessels or MBVSMCs was isolated using TRIzol reagent according to the manufacturer's instructions. 1 μg of RNA was reverse-transcribed to cDNA according to the manufacturer's instructions (Thermo Fisher Scientific Inc.). PCR reaction was performed using Fast SYBR® Green Master Mix Kit (Applied Biosystems, CA, USA). 18S rRNA was used as an endogenous control. The specific primer sequences of FBW7 and 18S rRNA were synthesized and provided by the Shanghai Biological Engineering Technology Services Co. Ltd. (Shanghai, China): FBW7 sense 5'-TGTCTGTCACTCGCCTACCA-3′ and antisense 5'-TTGAGTTACGGCTCCTGGTG-3′; Nox1 sense 5'-TTTT GCTGGCTGACACTTGC-3′ and antisense 5'-AGTGGGAAGCTTGGTCG TTC-3′; 18S rRNA sense, 5'-CGGCTACCACATCCAAGGAA-3′ and 5'-CTGGAATTACCGCGGCT-3′. Relative expression was determined using 18 s rRNA as an internal control and reported as $2^{-\Delta\Delta CT}$.

### 2.9. Cell proliferation assay

Cell viability was determined using Cell Counting Kit-8 (CCK-8; Yiyuan Biotechnology, Guangzhou, China) in accordance with the manufacturer's instructions. 10 μL of the CCK-8 reagent was added the cells and incubated for 4 h, at 37 °C, 5% $CO_2$. The absorbance value was read at 450 nm using SPECTRA MAX190 spectrophotometry (Sunnyvale, CA, USA). Cell proliferation was measured by the incorporation of BrdU during DNA synthesis. MBVSMCs were treated with 50 mmol/L BrdU for 4 h at 37 °C and then fixed with 4% paraformaldehyde and permeabilized with 2% HCI and 0.4% Triton X-100 for 15 min. After incubation of BrdU antibody (1:100, Santa Cruz) at 4 °C overnight, the cells were treated with biotinylated goat anti-mouse IgG antibody (1:200, Santa Cruz) for 1 h. The percentage of BrdU-positive cells was calculated by counting the numbers of stained cells and total cells.

### 2.10. Wound healing assay

The migration of MBVSMCs was assessed by wound healing assay. A sterile micropipette tip was used to create a 'wound' in the cell monolayers. 48 h later, the wound area was observed using a light microscope (CKX41). The width of each wound was measured using ImageJ software. Cell migration was presented as a percentage of the initial wound distance.

### 2.11. Invasion assay

The invasion of MBVSMCs was determined using a Transwell® chamber with 6.5-mm pore-size polycarbonate filter membrane (Costar, MA, USA). $1 \times 10^5$ MBVSMCs were seeded in the upper compartment and cultured in 100 μL medium containing 0.5% FBS. The lower compartment of the chamber contained 100 μL medium supplemented 20% FBS as a chemoattractant. After 48 h incubation, the invaded cells were fixed with 4% paraformaldehyde and stained with 1% crystal violet for 30 min. Cell invasion was imaged by a light microscope (CKX41) and quantified using ImageJ software.

### 2.12. Statistical analysis

All data were given as mean ± SEM. n value represented the number of mice or batches of cells. Comparisons between groups were analyzed using Student's *t*-test or one-way ANOVA with post hoc Tukey's test. The regression analysis was determined by the Pearson correlation test. Value of $P < .05$ was considered to be statistically significant.

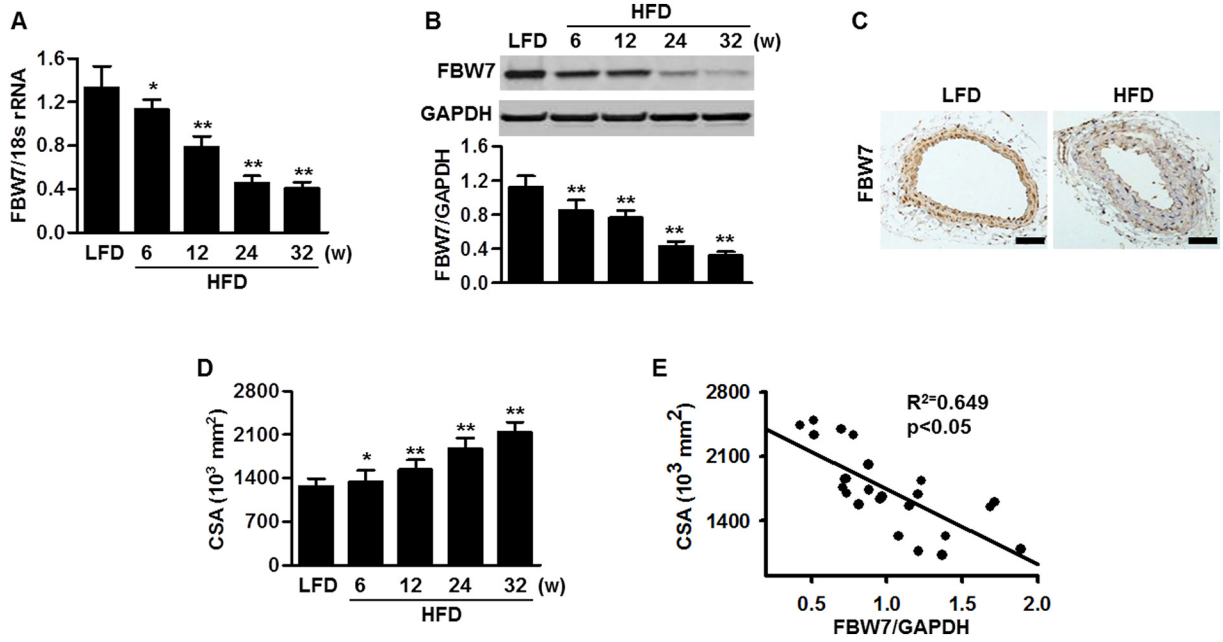


**Fig. 1.** Decreased expression of FBW7 in mouse brain microvessels during ICAS. (A) RT-PCR analysis for the mRNA level of FBW7 in brain microvessels from low fat diet (LFD)-fed ApoE$^{-/-}$ mice and high fat diet (HFD)-fed ApoE$^{-/-}$ mice at different time points (6, 12, 24, and 32 weeks) after HFD administration. (B) The protein expression of FBW7 was detected by western blotting. *$P < .05$, **$P < .01$ vs. LFD, $n = 6$ in each group. (C) Representative images of immunochemical staining for FBW7 expression in middle cerebral artery (MCA) from ApoE$^{-/-}$ mice after 32 weeks of LFD or HFD treatment. Scale bars: 100 μm. (D) Bar graph indicates the degree of MCA stenosis evaluated by cross sectional area (CSA). *P < .05, **P < .01 vs. LFD, n = 6 in each group. (E) Correlation between CSA value and FBW7 expression was analyzed.

## 3. Results

### 3.1. HFD-induced the MCA remodeling was negatively associated with FBW7 expression

As displayed in Fig. 1A, in mouse brain microvessels, the mRNA level of FBW7 was gradually decreased after HFD administration in a time-dependent manner. Western blotting revealed that the protein expression of FBW7 was significantly inhibited in HFD-fed mice compared with LFD-fed mice (Fig. 1B). Similar to the results of RT-PCR and western blotting, immunohistochemistry further confirmed the down-regulation of FBW7 in MCA isolation from HFD-fed mice, accompanied by a marked remodeling (Fig. 1C). HFD administration gradually increased the media thickness and decreased the lumen diameter, resulting in enhanced media CSA, which is a typical feature of vascular remodeling (Fig. 1D). Moreover, the reduced FBW7 expression was negatively correlated with the value of CSA with the correlation coefficient ($R^2$) of 0.649 (Fig. 1E). These results indicate that the alteration of FBW7 expression may be involved in ICAS.

### 3.2. Loss of FBW7 in SMCs exacerbated HFD-induced MCA remodeling and MBVSMC proliferation

To assess the role of FBW7 in cerebrovascular remodeling induced by atherosclerosis, we generated FBW7 SMC-specific knockout mice by breeding animals harboring FBW7-floxed allele with mice that express Cre from a SM22α promoter. The genotyping and protein expression of FBW7 were monitored by RT-PCR and western blotting, respectively. In MBVSMCs, FBW7 protein expression was almost abolished in FBW7$^{SMCKO}$ mice, but not in FBW7$^{f/f}$ mice (Fig. S1). Under the LFD-treated conditions, FBW7 deficiency slightly increased the level of TG, TC and CHO. After 32 weeks of HFD, plasma TG, LDL and CHO levels were significantly elevated, while the level of HDL was decreased. These alterations of lipid files were more pronounced in FBW7$^{SMCKO}$ mice than in FBW7$^{f/f}$ mice (Fig. 2A-D). Oil red O staining showed that SMC-specific knockout of FBW7 enhanced lipid accumulation in MCA (Fig. 2E). Hematoxylin and eosin staining of MCA of FBW7$^{SMCKO}$ mice showed significant remodeling compared with FBW7$^{f/f}$ mice under HFD administration, as evidenced by increased media CSA value (Fig. 2F). In addition, immunofluorescence of SMC marker α-SMA revealed that knockout of FBW7 further enhanced HFD-induced the increase in α-SMA fluorescence intensity and MCA media thickness (Fig. 2G), suggesting that the excessive SMC proliferation may contribute the cerebrovascular remodeling. We thus investigated the effect of FBW7 deficiency on MBVSMC proliferation. Although FBW7 knockout had no obvious effect on cell viability under LFD treatment, HFD-induced the increase of cell viability was greater in MBVSMC isolated from FBW7$^{SMCKO}$ mice than those from FBW7$^{f/f}$ mice (Fig. 2H). BrdU incorporation also supported that FBW7 knockout promoted HFD-induced MBVSMC proliferation (Fig. 2I). Given that SMC motility plays an important role in cerebrovascular remodeling (Dzau et al., 2002), the effects of FBW7 deficiency on MBVSMC migration and invasion were examined. As displayed in Fig. 2J, HFD markedly induced the ability of the cells to close the wound. Knockout of FBW7 augmented the effect of HFD on cell migration. Moreover, the Transwell invasion assay, an alternative assay for determining cell movement, showed that FBW7 deficiency further increased the number of invaded cells induced by HFD (Fig. 2K). Collectively, these data suggest that SMC-specific knockout of FBW7 promotes cerebrovascular SMC proliferation, migration and invasion, which may underlie the enhanced effects of FBW7 deficiency on ICAS.

### 3.3. FBW7 deficiency potentiated the HFD-induced NADPH oxidase-dependent oxidative stress

Increasing studies have demonstrated that oxidative stress is critical for vascular injury and ICAS (Wu et al., 2018; Forstermann, 2008; Zhao et al., 2015; Shen et al., 2018; Dong et al., 2019). Under LFD treatment conditions, ROS generation assessed with $H_2$DCF-DA was comparable in MCA between FBW7$^{f/f}$ mice and FBW7$^{SMCKO}$ mice. After a 32-week HFD

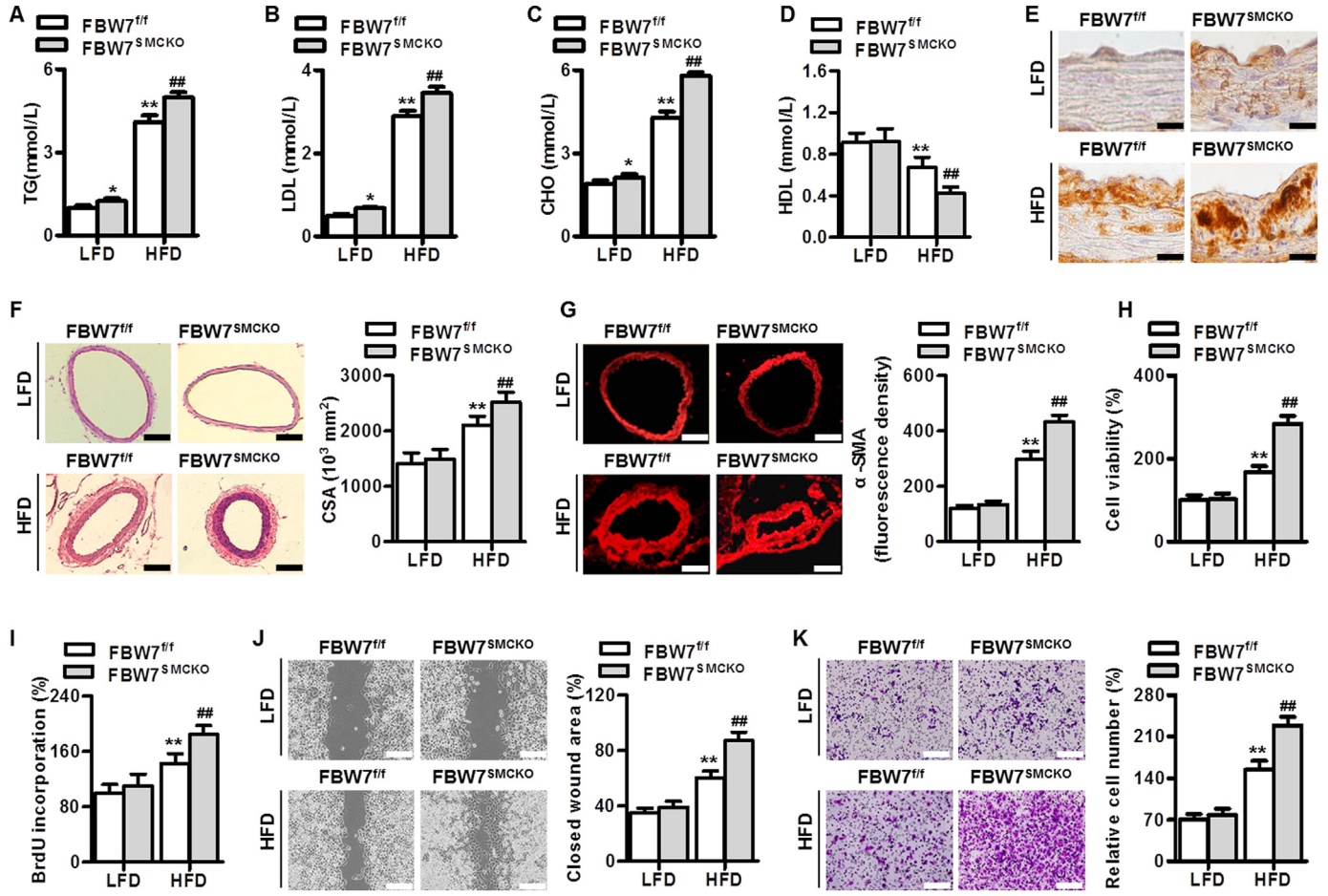


**Fig. 2.** Smooth muscle cell-specific loss of FBW7 aggravated ICAS. (A-D) Plasma triglyceride (TG), low-density lipoprotein (LDL), cholesterol (CHO) and high-density lipoprotein (HDL) of $FBW7^{f/f}$ mice or $FBW7^{SMCKO}$ mice on LFD or HFD for 32 weeks. *P < .05, **P < .01 vs. $FBW7^{f/f}$ LFD, ##P < .01 vs. $FBW7^{f/f}$ HFD, n = 6 in each group. (E) The lipid droplets in MCA were observed by oil red O staining. $n = 4$ in each group. Scale bars: 20 μm. (F) Representative images of hematoxylin and eosin staining of MCA. The degree of MCA stenosis was evaluated by CSA. Scale bars: 100 μm. (G) Representative images of immunofluorescence staining for α-SMA expression. Bar graph indicates the relative fluorescence density values for α-SMA expression. Scale bars: 100 μm. (H and I) Cell viability assay (H) and BrdU incorporation (I) were performed in mouse brain vascular smooth muscle cells (MBVSMCs) isolated from $FBW7^{f/f}$ mice or $FBW7^{SMCKO}$ mice on LFD or HFD for 32 weeks. (J and K) Cell motility was assessed by wound healing assay (J) and transwell analysis (K), respectively. Scale bars: 100 μm. **P < .01 vs. $FBW7^{f/f}$ LFD, ##P < .01 vs. $FBW7^{f/f}$ HFD, $n$ = 5–8 in each group. (For interpretation of the references to colour in this figure legend, the reader is referred to the web version of this article.)

administration, the fluorescence was significantly increased, and this increase was markedly potentiated in $FBW7^{SMCKO}$ mice (Fig. 3A). Consistently, FBW7 deficiency also enhanced HFD-induced increase in $O_2^-$ generation (Fig. 3B). The level of MDA in brain microvessels of HFD-fed $FBW7^{SMCKO}$ mice was significantly higher than those in HFD-fed $FBW7^{f/f}$ mice (Fig. 3C). However, the endogenous antioxidant enzymes, such as GPx and SOD, were further decreased in $FBW7^{SMCKO}$ mice (Fig. 3D and E). To distinguish the involvement of two major sources of ROS generation, NADPH oxidase and mitochondria-derived ROS, in FBW7-potentiated oxidative stress, NADPH oxidase activity and mROS generation were examined, respectively. After a HFD administration, both NADPH oxidase activity and mROS generation were significantly increased. The increase of NAPDH oxidase activity in brain microvessels was more pronounced in $FBW7^{SMCKO}$ mice than in $FBW7^{f/f}$ mice, but the increased mROS generation in MCA did not differ between $FBW7^{SMCKO}$ mice and their control mice (Fig. 3F and Fig. S3A). Furthermore, similar results were observed in MBVSMCs isolated from there four groups. In $FBW7^{SMCKO}$ cells, the oxidative stress induced by HFD was significantly exacerbated compared with $FBW7^{f/f}$ cells (Fig. S2A-E). Loss of FBW7 markedly potentiated the increase of NADPH oxidase activity in MBVSMCs, but also had no effect on the elevation of mROS generation induced by HFD (Fig. S2F and Fig. S3B). The results indicate that FBW7 may specifically regulate the function of NADPH oxidase.

### 3.4. Blockade of NADPH oxidase activity blunted the effects of FBW7 deficiency on MCA remodeling

To verify the role of NADPH oxidase in FBW7 deficiency-potentiated MCA remodeling, NADPH oxidase-specific inhibitor apocynin was used. Histological examination showed that FBW7 knockout-induced the MCA remodeling was significantly ameliorated after apocynin treatment (Fig. 4A and B). In MBVSMCs from $FBW7^{SMCKO}$ mice under HFD conditions, the increase of cell proliferation was abolished by apocynin (Fig. 4C and D). In addition, administration with apocynin largely abrogated the enhanced effects of FBW7 deficiency on MBVSMC migration and invasion (Fig. 4E and F). These results suggest that NADPH oxidase is indispensable for FBW7 deficiency in aggravating ICAS.

### 3.5. Nox1 was required for the effect of FBW7 deficiency on ICAS

NADPH oxidase complex is composed of membrane subunits (e.g. Nox family and p22phox) and cytosolic subunits (e.g. p47phox and p67phox) (Noubade et al., 2014). It has been demonstrated that VSMCs

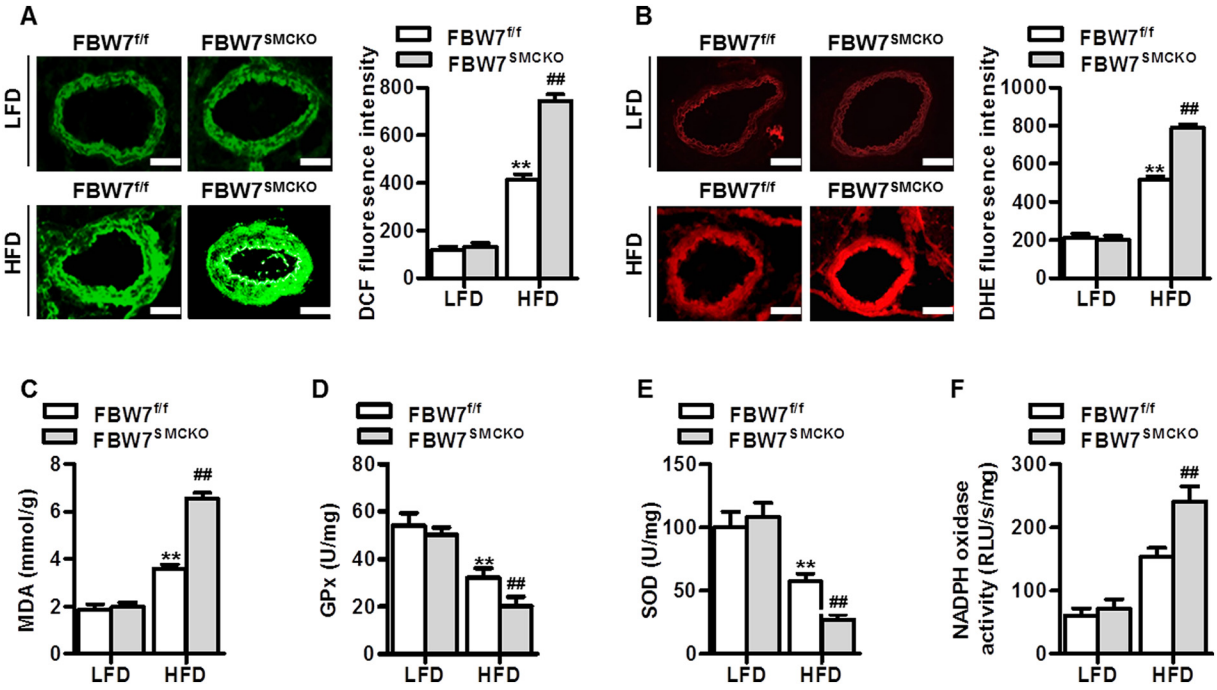


**Fig. 3.** FBW7 knockout exacerbated HFD-induced oxidative stress in brain microvessels. (A) Reactive oxygen species (ROS) generation in MCA sections was determined by $H_2$DCF-DA staining. Quantitative analysis of DCF fluorescence intensity. Scale bars: 100 μm. (B) Superoxide anion ($O_2^-$) was examined by dihydroethidium (DHE) staining. Quantitative evaluation of DHE fluorescence intensity was performed. Scale bars: 100 μm. (C–F) The levels of malondialdehyde (MDA) (C), glutathion peroxidase (GPx) (D), superoxide dismutase (SOD) (E) and NADPH oxidase activity (F) in homogenates of brain microvessles were measured. **P < .01 vs. $FBW7^{f/f}$ LFD, ##P < .01 vs. $FBW7^{f/f}$ HFD, n = 4–6 in each group.

mainly express the Nox2 homologues Nox1, not Nox2 (Martyn et al., 2006). When the expressions of these subunits were examined, the phosphorylation of p47phox and p67phox and the expression of Nox1 in brain microvessles were significantly elevated after HFD treatment. The increased phosphorylation of p47phox and p67phox were comparable between $FBW7^{f/f}$ mice and $FBW7^{SMCKO}$ mice. The expression of p22phox remained unchanged across treatment conditions. Interestingly, in $FBW7^{SMCKO}$ mice, the increase of Nox1 expression was further

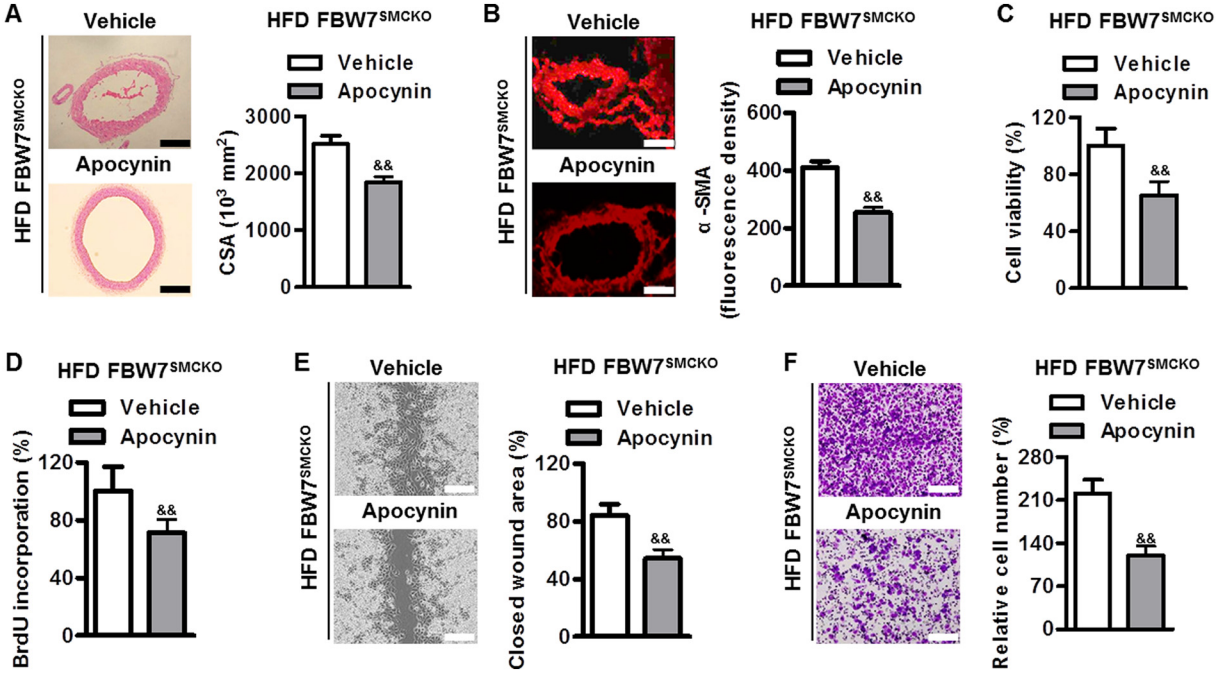


**Fig. 4.** Inhibition of NADPH oxidase activity improved FBW7 deficiency-potentiated ICAS under HFD-fed conditions. (A) Apocynin was injected intraperitoneally at a dose of 5 mg/kg in $FBW7^{SMCKO}$ mice after 6-week HFD administration. Representative images of hematoxylin and eosin staining of MCA was shown and the value of CSA was calculated. Scale bars: 100 μm. (B) Immunofluorescence staining for α-SMA expression. Bar graph indicates the relative fluorescence density value for α-SMA expression. Scale bars: 100 μm. (C and D) MBVSMC proliferation was examined by CCK-8 assay (C) and BrdU incorporation (D). (E and F) Cell motility was assessed by wound healing assay (E) and transwell analysis (F), respectively. Scale bars: 100 μm. &&P < .01 vs. $FBW7^{SMCKO}$ HFD Vehicle, n = 4–6 in each group.

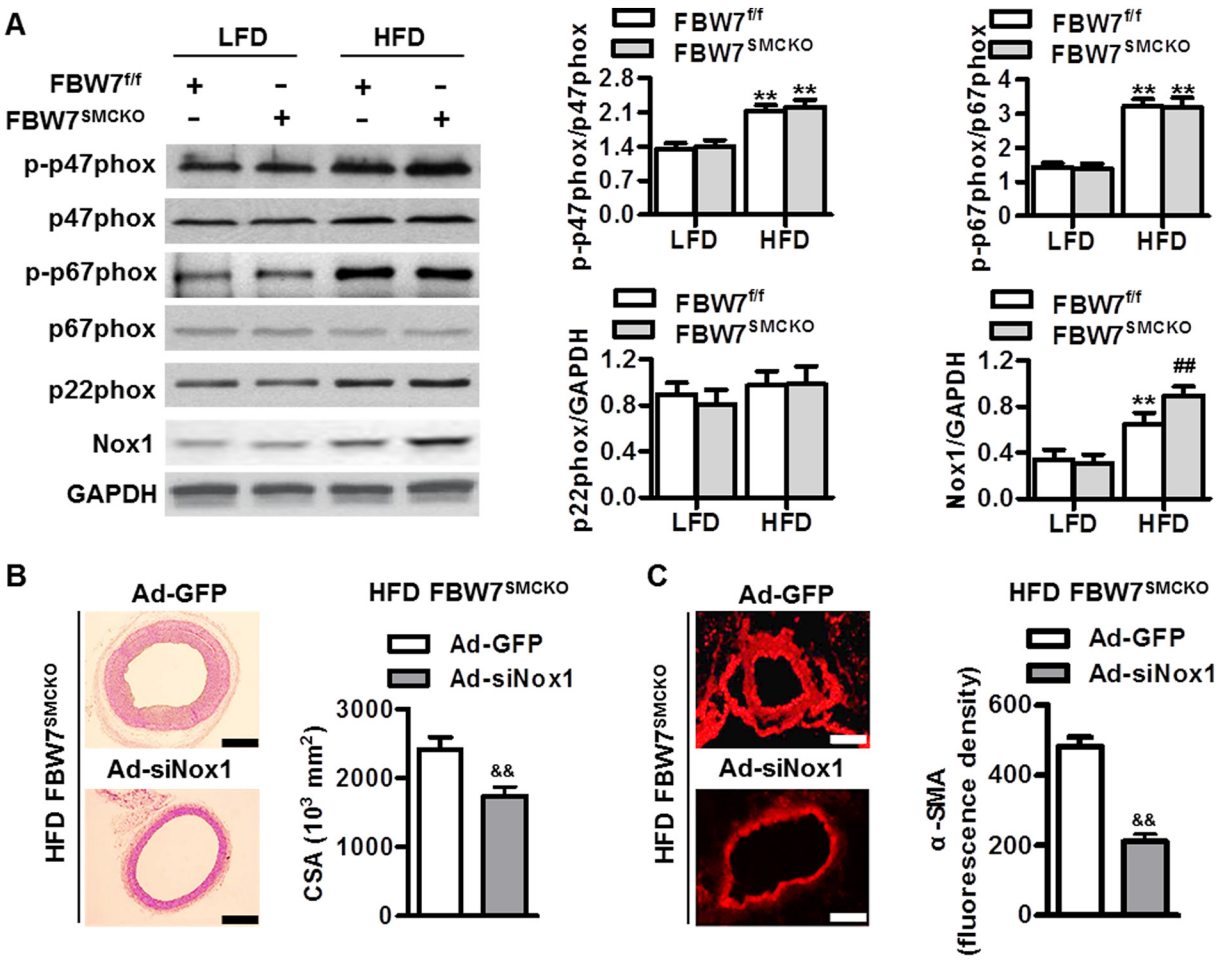


**Fig. 5.** Nox1 was indispensable for FBW7 deficiency in aggravating ICAS. (A) After 32 weeks of LFD or HFD treatment in FBW7$^{f/f}$ mice and FBW7$^{SMCKO}$ mice, western blot analysis of phosphorylation of p47phox and p67phox and expression of p22phox and Nox1 in the lysates of brain microvessels. **P < .01 vs. FBW7$^{f/f}$ LFD, ##P < .01 vs. FBW7$^{f/f}$ HFD, n = 5 in each group. (B) FBW7$^{SMCKO}$ mice were administrated with HFD for 24 weeks and then injected with $5.0 \times 10^{10}$ vp of Ad-GFP or Ad-siNox1 via tail vein for 8 weeks under HFD treatment. Hematoxylin and eosin staining of MCA. Scale bars: 100 μm. (C) Immunofluorescence staining for α-SMA expression. Scale bars: 100 μm. &&P < .01 vs. FBW7$^{SMCKO}$ HFD Ad-GFP, n = 5 in each group.

enhanced, indicating that Nox1 may be the key molecular target of FBW7 in regulating ROS generation (Fig. 5A). To further explore the functional role of Nox1 in FBW7 deficiency-potentiated MCA remodeling, HFD-fed FBW7$^{SMCKO}$ mice were infected with Ad-siNox1 to downregulate the expression of Nox1 (Fig. S4). As displayed in Fig. 5B and C, the increase of MCA remodeling induced by FBW7 deficiency was completely abolished by downregulation of Nox1. Collectively, the data indicate that the increase of Nox1 underlies at least partially the enhanced effects of FBW7 deficiency on MCA remodeling.

### 3.6. Deficiency of FBW7 prevented Nox1 degradation

To explore the mechanism how FBW7 regulates Nox1 expression, we initially tested the effect of FBW7 deficiency on Nox1 mRNA level. HFD treatment notably increased the mRNA level of Nox1 in brain microvessels and MBVSMCs, but this increase was comparable between FBW7$^{f/f}$ mice and FBW7$^{SMCKO}$ mice (Fig. S5). This excluded that the transcriptional regulation was involved. Immunoprecipitation clearly showed that FBW7 interacted with Nox1, and reciprocal interaction was further confirmed using FWB7 antibody (Fig. 6A and B). Considering the capacity of FBW7 to induce protein degradation, the protein stability of Nox1 was assessed using a protein synthesis inhibitor cycloheximide. Under HFD-treated conditions, treatment of MBVSMCs with cycloheximide showed a time-dependent decrease of Nox1 protein expression. Compared with FBW7$^{f/f}$ mice, loss of FBW7 markedly antagonized against the degradation of Nox1, prolonging the protein half-life of Nox1 by > 11 h (Fig. 6C). Additionally, HFD administration decreased the level of Nox1 ubiquitination in brain microvessels, and the decrease in Nox1 ubiquitination was dramatically potentiated by knockout of FBW7 (Fig. 6D). This result was confirmed in MBVSMCs (Fig. 6E). Overall, these data suggest that FBW74 deficiency promotes the increase in Nox1 expression by inhibiting ubiquitin-mediated degradation.

## 4. Discussion

This study unveils a link between FBW7 and NADPH oxidase-mediated oxidative stress in the pathogenesis of MCA remodeling. In response to a challenge with HFD, FBW7 expression is decreased in brain arteries and directly interacts with Nox1, leading to the reduced Nox1 degradation. The increased Nox1 level further aggravates NADPH oxidase activity and oxidative stress, which contribute to lipid accumulation and VSMC proliferation, thereby promoting ICAS development (Fig. 6F).

Protein ubiquitination, a highly conserved process, is triggered by binding an ubiquitin molecule to a lysine residue of the target substrate protein via three enzymatic proteins: the ubiquitin-activating enzyme E1, the ubiquitin-conjugating enzyme E2, and the ubiquitin ligase E3 (Ordureau et al., 2015). Among these enzymatic proteins, E3 ligases control the specificity of ubiquitination cascade (Ordureau et al., 2015).

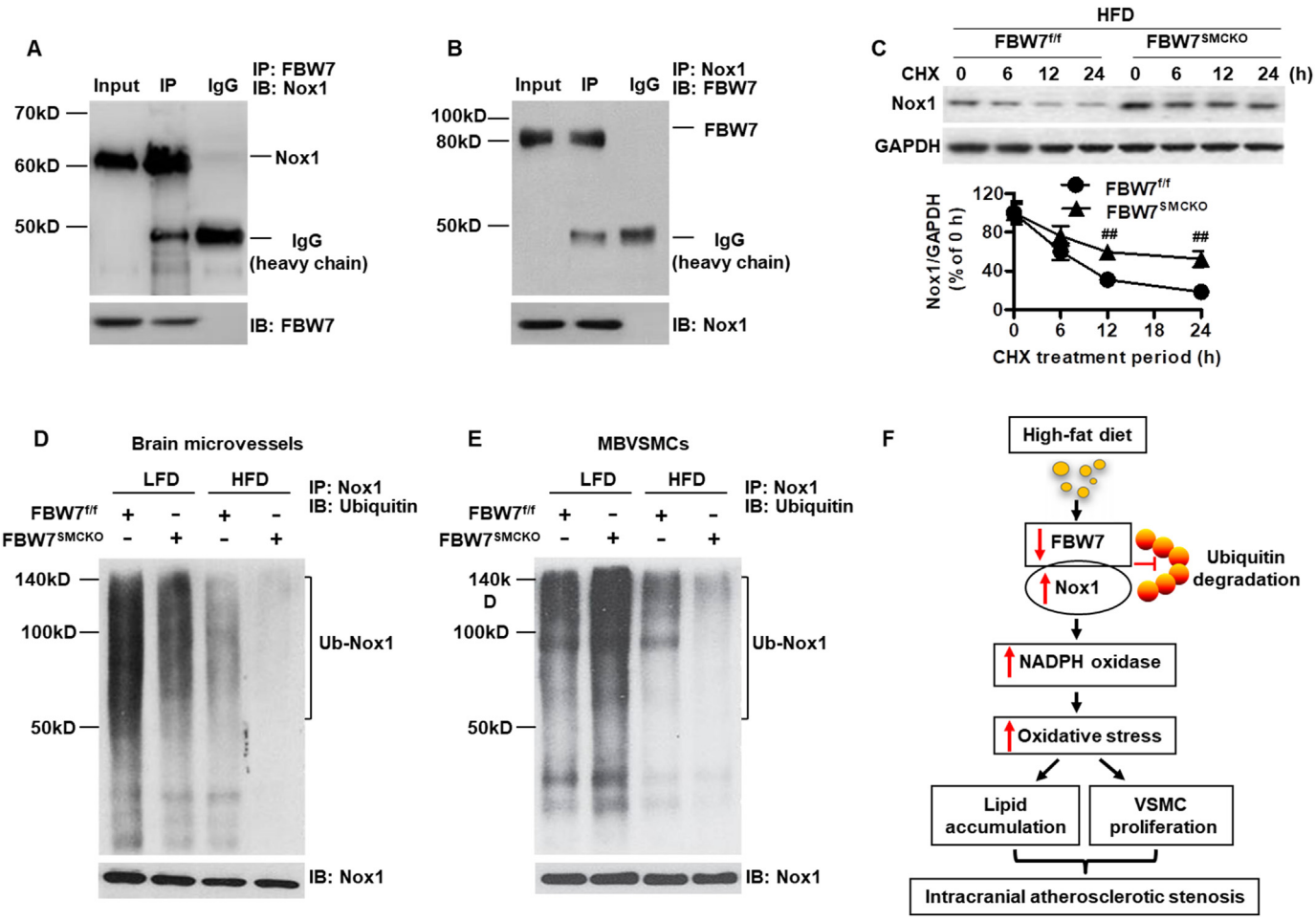


**Fig. 6.** FBW7 interacted with Nox1 and regulates its degradation. (A) Brain microvessels lysates were immunoprecipitated (IP) with FBW7 antibody and immunoprecipitated proteins were immunoblotted (IB) with Nox1 antibody. (B) The lysates were immunoprecipitated with Nox1 antibody and immunoprecipitated proteins were blotted with FBW7 antibody. (C) The MBVSMCs from HFD-fed $FBW7^{f/f}$ mice or HFD-fed $FBW7^{SMCKO}$ mice were incubated with cycloheximide (CHX, 10 μg/mL) for the indicated times. Nox1 protein expression was examined by western blotting. ##P < .01 vs. $FBW7^{f/f}$ HFD, n = 5 in each group. (D and E) Brain microvessels (D) or MBVSMCs lysates (E) from each group were immunoprecipitated with Nox1 antibody and blotted with ubiquitin antibody. n = 4 in each group. (F) Schematic illustration of cellular and molecular events underlying SMC FBW7-regulated intracranial atherosclerotic stenosis.

Emerging evidences have showed that pathological alteration of E3 ligases or E3 ligases-mediated ubiquitination plays a very important role in the development of atherosclerosis. For example, Nedd4 deficiency in VSMCs promoted atherosclerotic calcification by stabilizing pSmad1 (Lee et al., 2017). Itch directly modulated SIRT6 and SREBP2 ubiquitination, which are crucial for lipid metabolism and atherosclerosis (Stohr et al., 2015). Although previous studies have suggested that FBW7 is required for vascular development, the information related to FBW7 in cardiovascular system is very limited (Tsunematsu et al., 2004; Tetzlaff et al., 2004). Until recently, a finding reported by Zheng et al. revealed that KLF5 and FBW7 may cooperatively promote atherosclerotic development (Zheng et al., 2018). Here, we investigated the role of FBW7 in brain microvessels and the results showed that FBW7 expression was gradually decreased during MCA remodeling. Additionally, the reduced FBW7 expression was negatively correlated with the degree of remodeling, indicating FBW7 may have a role in intracranial stenosis.

There are two kinds of vascular remodeling, positive remodeling and negative remodeling (Burke et al., 2002). Positive remodeling results in enlargement of vessels, which is more commonly seen in basilar artery due to large plaque formation (Burke et al., 2002; Ma et al., 2010). On the other hand, negative remodeling is usually associated with inner-diameter narrowing due to VSMC proliferation and commonly found in MCA (Zhang et al., 2017; Burke et al., 2002). Indeed, HR-MRI analysis for the characteristics of MCA showed a significant intima media thickening in ischemic stroke (Zhang et al., 2017). Thus, in this study, we mainly observed the effect of FBW7 on MCA stenosis. Because FWB7 global knockout mice die around 10.5 days post coitus for deficiencies in vascular development and heart chamber maturation (Tetzlaff et al., 2004), we generated SMC-specific FBW7 knockout mice and found that $FBW7^{SMCKO}$ mice had no clear phenotype under normal physiological conditions. More importantly, our results identified a negative role of VSMC FBW7 in MCA remodeling. It is worth noting that the thickened intima is mainly composed of VSMCs (Takekawa et al., 2004). The proliferating VSMCs migrate from the media to intima and induce extracellular matrix production, leading to enhanced neointima (Dzau et al., 2002). Accordingly, we found that FBW7 deficiency markedly potentiated MBVSMC proliferation and migration.

Despite numerous factors contribute to VSMC proliferation, oxidative stress is still considered as the major underlying mechanism (Dzau et al., 2002; Zhao et al., 2015; Dong et al., 2019). Administration with antioxidant NAC effectively limited angiotensin II-induced the proliferation of primary rat VSMCs (Zhao et al., 2015). Inhibition NADPH oxidase-mediated ROS generation ameliorated cerebrovascular remodeling (Dong et al., 2019). We found that FBW7 deficiency exacerbated HFD-induced oxidative stress in brain microvessles and MBVSMCs. This observation was in line with a previous study that FBW7 restrained ROS generation and subsequently ensured terminal

maturation of bone marrow erythroid cells (Xu et al., 2014). NADPH oxidase and mitochondrial electron transport chain are the major sources of intracellular ROS (Forstermann, 2008). Interestingly, HFD-induced the increase in NADPH oxidase activity was augmented by knockout of FBW7, while the increased mROS generation was comparable between $FBW7^{SMCKO}$ mice and their control mice. This may exclude the involvement of mROS. Additionally, the NADPH oxidase inhibitor apocynin abolished the effect of FBW7 deficiency on VSMC proliferation, migration and MCA remodeling, further supporting that NADPH oxidase is required for FBW7-potentiated VSMC hyperplasia and MCA remodeling.

NADPH oxidase is activated by phosphorylation of cytosolic subunits (such as p47phox and p67phox) translocating to interact with membrane subunits (such as p22phox and Nox2/gp91phox) (Shen et al., 2018; Noubade et al., 2014). These subunits have different abundance and capacity to produce ROS in specific cell type. Notably, Nox2 is highly expressed in endothelial cells, but not in VSMCs (Zhao et al., 2015; Lassegue et al., 2001). However, the homologues of Nox2, Nox1 shares 56% similarity with NOX2 and is mainly expressed in VSMCs (Martyn et al., 2006). Our results revealed that the effect of FBW7 deficiency on NADPH oxidase activity was not associated with any difference in the phosphorylation of p47phox and p67phox as well as the expression of p22phox. Nevertheless, the increased expression of Nox1 was significantly enhanced, suggesting that Nox1 likely accounts for the contribution of FBW7 deficiency to NADPH oxidase activity. Furthermore, the effect of FBW7 deficiency on MCA remodeling was completely abolished after Nox1 downregulation. Surprisingly, loss of FBW7 did not affect the mRNA level of Nox1. Considering the capacity of FBW7 to cause protein degradation, we accordingly determined the protein stability of Nox1. The results clearly showed that FBW7 deficiency markedly inhibited Nox1 degradation. Although a previous study showed that PGC-1α modulated Nox1 degradation in VSMCs (Zhao et al., 2015), the direct E3 ubiquin ligases for Nox1 have not been reported. We reported for the first time that Nox1 is a novel FBW7-interacting protein and functions as a substrate of FBW7. Thus, knockout of FBW7 inhibits Nox1 ubiquitination and degradation, leading to potentiated Nox1-containing NADPH oxidase activity.

There are some limitations in the present study. Firstly, age is critically associated with the development of ICAS. Whether the development of ICAS in HFD-fed $FBW7^{SMCKO}$ mice is age dependent remains to be explored. Secondly, ICAS is one of the major contributors to ischemic stroke, however, the effect of FBW7 on ischemic stroke was not examined. Thirdly, we did not set a positive control throughout the study. Finally, we used brain microvessels or MBVSMCs in the study of mechanism due to lack of protein amount of MCA, although the morphological data demonstrated that SMC-specific deficiency of FBW7 exacerbated MCA stenosis. The MBVSMCs from microvessels may be not fully representative that from the larger vessel, such as MCA remodeling. Thus, further research is indispensable to better understand the specific role of FBW7 in ICAS to finally conclude if FBW7 can be functioned as an effective modulator in ICAS-related stroke treatment.

In conclusion, our study demonstrates that FBW7 knockout in VSMCs prevents the ubiquitin-mediated degradation of Nox1, which in turn aggravates MCA remodeling through enhancing NAPDH oxidase activity and ROS generation. These findings suggest that FBW7 may be a novel molecular target for the treatment of ICAS.

## Declaration of Competing Interest

The authors declare that they have no conflict of interest.

## Acknowledgement

This study was supported by the Torch Research Fund from the Fourth Affiliated Hospital of Harbin Medical University (HYDSYHJ201901).

## Appendix A. Supplementary data

Supplementary data to this article can be found online at https://doi.org/10.1016/j.nbd.2019.104584.

## References

Biswas, M., Phan, D., Watanabe, M., Chan, J.Y., 2011. The Fbw7 tumor suppressor regulates nuclear factor E2-related factor 1 transcription factor turnover through proteasome-mediated proteolysis. J. Biol. Chem. 286 (45), 39282–39289. https://doi.org/10.1074/jbc.M111.253807.

Burke, A.P., Kolodgie, F.D., Farb, A., Weber, D., Virmani, R., 2002. Morphological predictors of arterial remodeling in coronary atherosclerosis. Circulation 105 (3), 297–303.

Chen, D., Zang, Y.H., Qiu, Y., Zhang, F., Chen, A.D., Wang, J.J., Chen, Q., Li, Y.H., Kang, Y.M., Zhu, G.Q., 2019. BCL6 attenuates proliferation and oxidative stress of vascular smooth muscle cells in hypertension. Oxidative Med. Cell. Longev. 2019, 5018410. https://doi.org/10.1155/2019/5018410.

Chimowitz, M.I., Lynn, M.J., Howlett-Smith, H., Stern, B.J., Hertzberg, V.S., Frankel, M.R., Levine, S.R., Chaturvedi, S., Kasner, S.E., Benesch, C.G., Sila, C.A., Jovin, T.G., Romano, J.G., Warfarin-Aspirin Symptomatic Intracranial Disease Trial I, 2005. Comparison of warfarin and aspirin for symptomatic intracranial arterial stenosis. N. Engl. J. Med. 352 (13), 1305–1316. https://doi.org/10.1056/NEJMoa043033.

Chimowitz, M.I., Lynn, M.J., Derdeyn, C.P., Turan, T.N., Fiorella, D., Lane, B.F., Janis, L.S., Lutsep, H.L., Barnwell, S.L., Waters, M.F., Hoh, B.L., Hourihane, J.M., Levy, E.I., Alexandrov, A.V., Harrigan, M.R., Chiu, D., Klucznik, R.P., Clark, J.M., McDougall, C.G., Johnson, M.D., Pride Jr., G.L., Torbey, M.T., Zaidat, O.O., Rumboldt, Z., Cloft, H.J., Investigators, S.T., 2011. Stenting versus aggressive medical therapy for intracranial arterial stenosis. N. Engl. J. Med. 365 (11), 993–1003. https://doi.org/10.1056/NEJMoa1105335.

Ciechanover, A., Orian, A., Schwartz, A.L., 2000. Ubiquitin-mediated proteolysis: biological regulation via destruction. BioEssays 22 (5), 442–451. https://doi.org/10.1002/(SICI)1521-1878(200005)22:5<442::AID-BIES6>3.0.CO;2-Q.

Davis, R.J., Gonen, M., Margineantu, D.H., Handeli, S., Swanger, J., Hoellerbauer, P., Paddison, P.J., Gu, H., Raftery, D., Grim, J.E., Hockenbery, D.M., Margolin, A.A., Clurman, B.E., 2018. Pan-cancer transcriptional signatures predictive of oncogenic mutations reveal that Fbw7 regulates cancer cell oxidative metabolism. Proc. Natl. Acad. Sci. U. S. A. 115 (21), 5462–5467. https://doi.org/10.1073/pnas.1718338115.

Dong, H., Ming, S., Fang, J., Li, Y., Liu, L., 2019. Icariin ameliorates angiotensin II-induced cerebrovascular remodeling by inhibiting Nox2-containing NADPH oxidase activation. Hum. Cell 32 (1), 22–30. https://doi.org/10.1007/s13577-018-0220-3.

Dzau, V.J., Braun-Dullaeus, R.C., Sedding, D.G., 2002. Vascular proliferation and atherosclerosis: new perspectives and therapeutic strategies. Nat. Med. 8 (11), 1249–1256. https://doi.org/10.1038/nm1102-1249.

Fois, A.G., Posadino, A.M., Giordo, R., Cossu, A., Agouni, A., Rizk, N.M., Pirina, P., Carru, C., Zinellu, A., Pintus, G., 2018. Antioxidant activity mediates Pirfenidone Antifibrotic effects in human pulmonary vascular smooth muscle cells exposed to sera of idiopathic pulmonary fibrosis patients. Oxidative Med. Cell. Longev. 2018, 2639081. https://doi.org/10.1155/2018/2639081.

Forstermann, U., 2008. Oxidative stress in vascular disease: causes, defense mechanisms and potential therapies. Nat. Clin. Pract. Cardiovasc. Med. 5 (6), 338–349. https://doi.org/10.1038/ncpcardio1211.

Gauthier, S.A., Sahoo, S., Jung, S.S., Levy, E., 2012. Murine cerebrovascular cells as a cell culture model for cerebral amyloid angiopathy: isolation of smooth muscle and endothelial cells from mouse brain. Methods Mol. Biol. 849, 261–274. https://doi.org/10.1007/978-1-61779-551-0_18.

Gorelick, P.B., Wong, K.S., Bae, H.J., Pandey, D.K., 2008. Large artery intracranial occlusive disease: a large worldwide burden but a relatively neglected frontier. Stroke 39 (8), 2396–2399. https://doi.org/10.1161/STROKEAHA.107.505776.

Han, X.B., Li, H.X., Jiang, Y.Q., Wang, H., Li, X.S., Kou, J.Y., Zheng, Y.H., Liu, Z.N., Li, H., Li, J., Dou, D., Wang, Y., Tian, Y., Yang, L.M., 2017. Upconversion nanoparticle-mediated photodynamic therapy induces autophagy and cholesterol efflux of macrophage-derived foam cells via ROS generation. Cell Death Dis. 8 (6), e2864. https://doi.org/10.1038/cddis.2017.242.

Lassegue, B., Sorescu, D., Szocs, K., Yin, Q., Akers, M., Zhang, Y., Grant, S.L., Lambeth, J.D., Griendling, K.K., 2001. Novel gp91(phox) homologues in vascular smooth muscle cells: nox1 mediates angiotensin II-induced superoxide formation and redox-sensitive signaling pathways. Circ. Res. 88 (9), 888–894.

Lee, J.H., Jeon, S.A., Kim, B.G., Takeda, M., Cho, J.J., Kim, D.I., Kawabe, H., Cho, J.Y., 2017. Nedd4 deficiency in vascular smooth muscle promotes vascular calcification by stabilizing pSmad1. J. Bone Miner. Res. 32 (5), 927–938. https://doi.org/10.1002/jbmr.3073.

Ma, N., Jiang, W.J., Lou, X., Ma, L., Du, B., Cai, J.F., Zhao, T.Q., 2010. Arterial remodeling of advanced basilar atherosclerosis: a 3-tesla MRI study. Neurology 75 (3), 253–258. https://doi.org/10.1212/WNL.0b013e3181e8e714.

Martyn, K.D., Frederick, L.M., von Loehneysen, K., Dinauer, M.C., Knaus, U.G., 2006. Functional analysis of Nox4 reveals unique characteristics compared to other NADPH oxidases. Cell. Signal. 18 (1), 69–82. https://doi.org/10.1016/j.cellsig.2005.03.023.

Noubade, R., Wong, K., Ota, N., Rutz, S., Eidenschenk, C., Valdez, P.A., Ding, J., Peng, I., Sebrell, A., Caplazi, P., DeVoss, J., Soriano, R.H., Sai, T., Lu, R., Modrusan, Z., Hackney, J., Ouyang, W., 2014. NRROS negatively regulates reactive oxygen species during host defence and autoimmunity. Nature 509 (7499), 235–239. https://doi.org/10.1038/nature13152.

Ordureau, A., Munch, C., Harper, J.W., 2015. Quantifying ubiquitin signaling. Mol. Cell

58 (4), 660–676. https://doi.org/10.1016/j.molcel.2015.02.020.
Prentice, H., Modi, J.P., Wu, J.Y., 2015. Mechanisms of neuronal protection against excitotoxicity, endoplasmic reticulum stress, and mitochondrial dysfunction in stroke and neurodegenerative diseases. Oxidative Med. Cell. Longev. 2015, 964518. https://doi.org/10.1155/2015/964518.
Qiu, L.L., Luo, D., Zhang, H., Shi, Y.S., Li, Y.J., Wu, D., Chen, J., Ji, M.H., Yang, J.J., 2016. Nox-2-mediated phenotype loss of hippocampal parvalbumin interneurons might contribute to postoperative cognitive decline in aging mice. Front. Aging Neurosci. 8, 234. https://doi.org/10.3389/fnagi.2016.00234.
Shen, J., Rastogi, R., Guan, L., Li, F., Du, H., Geng, X., Ding, Y., 2018. Omega-3 fatty acid supplement reduces activation of NADPH oxidase in intracranial atherosclerosis stenosis. Neurol. Res. 40 (6), 499–507. https://doi.org/10.1080/01616412.2018.1451290.
Stohr, R., Mavilio, M., Marino, A., Casagrande, V., Kappel, B., Mollmann, J., Menghini, R., Melino, G., Federici, M., 2015. ITCH modulates SIRT6 and SREBP2 to influence lipid metabolism and atherosclerosis in ApoE null mice. Sci. Rep. 5, 9023. https://doi.org/10.1038/srep09023.
Takekawa, Y., Umezawa, T., Ueno, Y., Sawada, T., Kobayashi, M., 2004. Pathological and immunohistochemical findings of an autopsy case of adult moyamoya disease. Neuropathology 24 (3), 236–242.
Tang, H., Shao, H., Yu, C., Hou, J., 2011. Mcl-1 downregulation by YM155 contributes to its synergistic anti-tumor activities with ABT-263. Biochem. Pharmacol. 82 (9), 1066–1072. https://doi.org/10.1016/j.bcp.2011.07.064.
Tetzlaff, M.T., Yu, W., Li, M., Zhang, P., Finegold, M., Mahon, K., Harper, J.W., Schwartz, R.J., Elledge, S.J., 2004. Defective cardiovascular development and elevated cyclin E and notch proteins in mice lacking the Fbw7 F-box protein. Proc. Natl. Acad. Sci. U. S. A. 101 (10), 3338–3345. https://doi.org/10.1073/pnas.0307875101.
Tsunematsu, R., Nakayama, K., Oike, Y., Nishiyama, M., Ishida, N., Hatakeyama, S., Bessho, Y., Kageyama, R., Suda, T., Nakayama, K.I., 2004. Mouse Fbw7/Sel-10/Cdc4 is required for notch degradation during vascular development. J. Biol. Chem. 279 (10), 9417–9423. https://doi.org/10.1074/jbc.M312337200.
Wang, L., Feng, W., Yang, X., Yang, F., Wang, R., Ren, Q., Zhu, X., Zheng, G., 2018. Fbxw11 promotes the proliferation of lymphocytic leukemia cells through the concomitant activation of NF-kappaB and beta-catenin/TCF signaling pathways. Cell Death Dis. 9 (4), 427. https://doi.org/10.1038/s41419-018-0440-1.
Wu, X., Zhang, H., Qi, W., Zhang, Y., Li, J., Li, Z., Lin, Y., Bai, X., Liu, X., Chen, X., Yang, H., Xu, C., Zhang, Y., Yang, B., 2018. Nicotine promotes atherosclerosis via ROS-NLRP3-mediated endothelial cell pyroptosis. Cell Death Dis. 9 (2), 171. https://doi.org/10.1038/s41419-017-0257-3.
Xu, Y., Swartz, K.L., Siu, K.T., Bhattacharyya, M., Minella, A.C., 2014. Fbw7-dependent cyclin E regulation ensures terminal maturation of bone marrow erythroid cells by restraining oxidative metabolism. Oncogene 33 (24), 3161–3171. https://doi.org/10.1038/onc.2013.289.
Yada, M., Hatakeyama, S., Kamura, T., Nishiyama, M., Tsunematsu, R., Imaki, H., Ishida, N., Okumura, F., Nakayama, K., Nakayama, K.I., 2004. Phosphorylation-dependent degradation of c-Myc is mediated by the F-box protein Fbw7. EMBO J. 23 (10), 2116–2125. https://doi.org/10.1038/sj.emboj.7600217.
Zhang, D.F., Chen, Y.C., Chen, H., Zhang, W.D., Sun, J., Mao, C.N., Su, W., Wang, P., Yin, X., 2017. A high-resolution MRI study of relationship between remodeling patterns and ischemic stroke in patients with atherosclerotic middle cerebral artery stenosis. Front. Aging Neurosci. 9, 140. https://doi.org/10.3389/fnagi.2017.00140.
Zhang, X., Zhou, Y., Ding, W., Zhang, R., Yan, S., Deng, Y., Gao, F., Lou, M., 2019a. TPO-Ab plays a role in arterial remodeling in patients with intracranial stenosis. Atherosclerosis 280, 140–146. https://doi.org/10.1016/j.atherosclerosis.2018.11.032.
Zhang, B., Bailey, W.M., McVicar, A.L., Stewart, A.N., Veldhorst, A.K., Gensel, J.C., 2019b. Reducing age-dependent monocyte-derived macrophage activation contributes to the therapeutic efficacy of NADPH oxidase inhibition in spinal cord injury. Brain Behav. Immun. 76, 139–150. https://doi.org/10.1016/j.bbi.2018.11.013.
Zhao, Q., Zhang, J., Wang, H., 2015. PGC-1alpha limits angiotensin II-induced rat vascular smooth muscle cells proliferation via attenuating NOX1-mediated generation of reactive oxygen species. Biosci. Rep. 35 (5). https://doi.org/10.1042/BSR20150112.
Zheng, B., Zheng, C.Y., Zhang, Y., Yin, W.N., Li, Y.H., Liu, C., Zhang, X.H., Nie, C.J., Zhang, H., Jiang, W., Liu, S.F., Wen, J.K., 2018. Regulatory crosstalk between KLF5, miR-29a and Fbw7/CDC4 cooperatively promotes atherosclerotic development. Biochim. Biophys. Acta Mol. basis Dis. 1864 (2), 374–386. https://doi.org/10.1016/j.bbadis.2017.10.021.